Pergamon

Int. J. Heat Mass Transfer. Vol. 41, No. 14, pp. 2157–2174, 1998

Printed in Great Britain
0017-9310/98 $19.00 + 0.00

PII: S0017-9310(97)00305-0

Double diffusive and Marangoni convection in a multi-cavity system

M. Z. SAGHIR†
Department of Mechanical Engineering, UAE University, Al-Ain, U.A.E.

M. HENNENBERG
Chimie-Physique, Faculté des Sciences, U.L.B., Belgium

and

M. R. ISLAM
Department of Chemical and Petroleum Engineering, UAE University, Al Ain, U.A.E.

(*Received* 16 *October* 1997)

Abstract—This paper numerically investigates the interaction between the Marangoni and the double diffusive convection in the Maxworthy [*Journal of Fluid Mechanics*, 1983, **128**, 259–282] set-up. The model consists of a two-cavity rectangular system in which the smaller cavity is located at the top left corner of the larger one. The larger cavity is filled with hot salty fluid while the smaller one contains cold fresh fluid. This problem is solved for two different cases: the first one contains a rigid upper cavity, thereby, eliminating the Marangoni effect, and the second one contains a free-surface upper cavity. For the latter case, the interaction between the Marangoni (thermal and solutal) and the double diffusive regimes is investigated in detail. Finite element modelling results indicate that salinity induces stronger convection than the thermal ones. For the case for which a free surface exists, thermal and solutal Marangoni convection further enhances the strength of the cellular flow. Numerical results agree qualitatively with the Maxworthy experiment. It is shown that the governing equations should be solved in the complete form and that the surface tension should be taken into consideration during the numerical analysis.

1. INTRODUCTION

When heat and species transfer exist within a fluid layer, the temperature and concentration gradients create a convection mode. This phenomenon is called double-diffusive convection. According to its dynamic characteristics, double diffusive convection can be categorised into fingering or a diffusive regime [1–4]. One example of the fingering regime is the hot salty fluid layer overlying a cold fresh fluid layer. Similarly, an example of the diffusive regime is a hot salty fluid layer (slower diffusion) is underlying a cold fresh fluid layer (faster diffusion). The latter case is the subject of our investigation.

Even though evidences indicate that double diffusive processes were observed centuries ago [5], the diffusive process during the motion of an intruding fluid remains one of the most elusive topics of fluid mechanics [6]. Thangam and Chen [7] were some of the first researchers to purposely devise an experiment to better understand double diffusive convections. They injected lighter salty water onto a heavier and colder body of salty water. While this experiment led to the observation of the salt finger convection, no quantitative results were reported. This problem of stable stratification that complicated the description of the current was remedied by Maxworthy [3] who devised a much simpler experiment to observe the double diffusive convection. He studied the intrusion of a sugar solution into a salt solution. The main reason for using salt and sugar was that the diffusivity of sugar is less than that of salt. Maxworthy [3] measured the spreading rates of the two-dimensional double diffusive intrusions and found that the transfer of mass and momentum across the sugar/salt interface dominates the motion of the intrusion. In his experimental set-up, although an air gap existed between the solution and the top plate, no Marangoni convection was observed. This absence may be due to the contamination at the free surface [8, 9]. However, no numerical experimentation has been reported to confirm or refute this postulate.

Yoshida *et al.* [10] repeated the Maxworthy work numerically without taking into consideration the Marangoni effects. In their analysis, cold/fresh water was released on to the ambient warm/salty water. They found that three parameters dominate the con-

† Author to whom correspondence should be addressed.

NOMENCLATURE

c	concentration of the fluid [%wt]	β_C	diffusive volume expansion [%wt^{-1}]
c_0	reference concentration of the fluid [%wt]	β_T	thermal volume expansion [C^{-1}]
C	non-dimensional concentration	Δc	initial concentration difference [%wt]
C_p	specific heat [cal g^{-1} C^{-1}]	ΔT	initial temperature difference [°C]
g	gravity vector [cm s^{-2}]	θ	non-dimensional temperature
k	conductivity [cal cm^{-1} s^{-1} C^{-1}]	μ	viscosity of the fresh water [g cm^{-1} s^{-1}]
L	characteristic length [cm]	ν	kinematic viscosity of the fresh water [cm^2 s^{-1}]
p	pressure [g cm^{-1} s^{-2}]	ρ	density of the fresh water [g cm^{-3}]
t	time [s]	σ_{m0}	surfacen tension at the reference temperature [dyne cm^{-1}]
T	temperature [°C]	τ	non-dimensional time
T_0	reference temperature [°C]	ψ	stream function.
u_0	reference velocity [cm s^{-1}]		
x, y	dimension [cm].		

Greek symbols

α_C	solutal diffusion coefficient

Subscript

0	reference value.

vection phenomenon. They are the turbulent Prandtl number, the turbulent thermal Rayleigh number and finally the Turner number. In their study, they used the Navier–Stokes equations for laminar regime. In their numerical analysis, they modified the mass transfer equation and introduced the density flux ratio. They ignored the influence of the free surface force in the flow. Also, by taking the vertical diffusion equal to the horizontal one, they simplified the problem considerably. As a consequence, no solutal Rayleigh number appears as an independent parameter in their work.

Hyun and Bergman [11] studied the double diffusive phenomenon for a two-layer system numerically. They concentrated their study to the interfacial behaviour between the two-layer systems and determined the critical Rayleigh number that leads to the destruction of the interface. Also, they reported vigorous fluctuations of temporal Nusselt numbers, indicating the existence of unstable flow regimes. However, no broad discussion was provided on the topic. No comment was made on the influence of the interfacial tension between the two fluid systems.

Chen and Su [12] conducted a linear stability analysis on a layer of stratified salt solution with a free surface heated from below. Results indicated that the onset of instability will occur at a much lower thermal Rayleigh number when reasonable surface tension gradient with respect to temperature and concentration are assumed. Tanny *et al.* [13] studied the effects of interaction between Marangoni and double-diffusive instabilities in a less contaminated system. In their experiment, a cavity filled with different salt concentrations was subject to a temperature difference between the top and the bottom plates. A small air gap at the top surface between the solution and the plate was created to allow the Marangoni effect to take place. They reported that at high initial solutal Rayleigh numbers ($Ra_C > 5.3\ 10^6$), Marangoni instabilities occur prior to the double diffusive instabilities. At lower initial solutal Rayleigh numbers ($Ra_C < 5.3\ 10^6$), both Marangoni and double diffusive instabilities occur simultaneously. Their experimental study was complimented with a stability analysis that showed reasonable agreement with experimental results.

The main objective of this paper is to examine numerically the interaction between the Marangoni and the double diffusive convection using the Maxworthy experimental set-up. Different parameters that influence the convection are studied. In particular, the importance of the Prandtl number, the Lewis number and finally the thermal and solutal Marangoni numbers are examined in detail. The complete Navier–Stokes equation was used without introducing the density flux ratio as in Yoshida *et al.* [10] case. Our numerical results reveal the physics behind the Maxworthy experiment and demonstrate the effectiveness of coupling the Marangoni effects with the double diffusive convection.

2. GOVERNING EQUATIONS AND NUMERICAL PROCEDURE

The complete Navier–Stokes equations together with the energy and the solutal equations were solved numerically using the finite element technique. The prototype modelled was the experimental set-up as reported by Maxworthy [3].

2.1. *Governing equations and boundary conditions*

The momentum balance equation was represented by the Navier–Stokes equation. In the x direction, the equation is written as follows:

$$\rho\left[\frac{\partial u}{\partial t}+u\frac{\partial u}{\partial x}+v\frac{\partial u}{\partial y}\right]=-\frac{\partial p}{\partial x}+\mu\left[\frac{\partial^2 u}{\partial x^2}+\frac{\partial^2 u}{\partial y^2}\right]. \quad (1)$$

In the y direction, the equation is written as:

$$\rho\left[\frac{\partial v}{\partial t}+u\frac{\partial v}{\partial x}+v\frac{\partial v}{\partial y}\right]=-\frac{\partial p}{\partial y}+\mu\left[\frac{\partial^2 v}{\partial x^2}+\frac{\partial^2 v}{\partial y^2}\right]$$
$$-\rho g[\beta_T(T-T_0)-\beta_C(c-c_0)]. \quad (2)$$

In the above equations, (u,v) are the velocity components in the x and y directions, respectively. The pressure is denoted by p, the temperature is T, the concentration is c and the density is ρ. The time is known by t, the thermal volume expansion is β_T, the solutal volume expansion is denoted by β_C, the viscosity is denoted by μ and g is the gravity constant. The mass conservation is written in the form of the continuity equation as follows:

$$\frac{\partial u}{\partial x}+\frac{\partial v}{\partial y}=0. \quad (3)$$

The energy balance equation is expressed as follows:

$$\rho C_p\left[\frac{\partial T}{\partial t}+u\frac{\partial T}{\partial x}+v\frac{\partial T}{\partial y}\right]=k\left[\frac{\partial^2 T}{\partial x^2}+\frac{\partial^2 T}{\partial y^2}\right] \quad (4)$$

where C_p is the specific heat, T the temperature and k is the conductivity of the fluid. Finally, the mass transfer equation for the solute is written as follows:

$$\left[\frac{\partial c}{\partial t}+u\frac{\partial c}{\partial x}+v\frac{\partial c}{\partial y}\right]=\alpha_C\left[\frac{\partial^2 c}{\partial x^2}+\frac{\partial^2 c}{\partial y^2}\right]. \quad (5)$$

In the above equation, c is the concentration or salinity of the fluid and α_C is the solutal diffusion coefficient. Equations (1)–(5) were rendered dimensionless by using the following dimensionless variables:

$$U=\frac{u}{u_0},\quad V=\frac{v}{u_0},\quad X=\frac{x}{L},\quad Y=\frac{y}{L},\quad P=\frac{p}{\rho u_0^2}$$
$$u_0=\sqrt{g\beta_T\Delta TL},\quad \tau=\frac{tu_0}{L},\quad \theta=\frac{T-T_0}{\Delta T},\quad C=\frac{c-c_0}{\Delta c} \quad (6)$$

where u_0 is a reference velocity (assumes $u_0 = 0.4427$ cm s^{-1} for a $\beta_T = 2\times10^{-4}$ C^{-1}, $\Delta T = 1$°C, $\Delta c = 1$, $L = 1$ cm and $g = 980$ cm s^{-2}), ΔT the initial temperature difference, and L is a characteristic length (see Fig. 1). Equations (1)–(5) in their dimensionless forms become as follows:

Navier–Stokes equations

x-direction

$$\left[\frac{\partial U}{\partial \tau}+U\frac{\partial U}{\partial X}+V\frac{\partial U}{\partial Y}\right]=-\frac{\partial P}{\partial X}+\frac{1}{\sqrt{Gr}}\left[\frac{\partial^2 U}{\partial X^2}+\frac{\partial^2 U}{\partial Y^2}\right]. \quad (7)$$

y-direction

$$\left[\frac{\partial V}{\partial \tau}+U\frac{\partial V}{\partial X}+V\frac{\partial V}{\partial Y}\right]=-\frac{\partial P}{\partial Y}+\frac{1}{\sqrt{Gr}}\left[\frac{\partial^2 V}{\partial X^2}+\frac{\partial^2 V}{\partial Y^2}\right]$$
$$-\left[\theta-\frac{\beta_C\Delta c}{\beta_T\Delta T}C\right] \quad (8)$$

where $Gr = (g\beta_T\Delta TL^3/\nu^2)$ is the Grashof number.

Continuity equation

$$\left[\frac{\partial U}{\partial X}+\frac{\partial V}{\partial Y}\right]=0. \quad (9)$$

Energy balance equation

$$\left[\frac{\partial \theta}{\partial \tau}+U\frac{\partial \theta}{\partial X}+V\frac{\partial \theta}{\partial Y}\right]=\frac{1}{\sqrt{Ra_T Pr}}\left[\frac{\partial^2 \theta}{\partial X^2}+\frac{\partial^2 \theta}{\partial Y^2}\right] \quad (10)$$

where $Pr = (C_p\mu/k)$ is the Prandtl number and $Ra_T = (g\beta_T\Delta TL^3/\nu\alpha)$ is the thermal Rayleigh number.

Mass balance equation

$$\left[\frac{\partial C}{\partial \tau}+U\frac{\partial C}{\partial X}+V\frac{\partial C}{\partial Y}\right]=\frac{1}{\sqrt{Ra_C Sc}}\left[\frac{\partial^2 C}{\partial X^2}+\frac{\partial^2 C}{\partial Y^2}\right] \quad (11)$$

where $Sc = (\mu/\rho\alpha_C)$ is the Schmidt number and $Ra_C = (g\beta_C\Delta cL^3/\nu\alpha_C)$ is the solutal Rayleigh number.

Figure 1 shows the model to be solved and the boundary conditions used in this analysis. It consists of a cavity having a width of 0.5 cm (W_1) and 1 cm long (L) enclosed in a cavity of 1 cm width (W_2) and 10 cm length (L_2). This model is a simple case of the Maxworthy [3] experimental model. The smaller cavity contains the cold fresh water known as being the faster diffusing solution and the bigger cavity contains the hot salted water known as the slower diffusing solution. At time $t = 0$, the fresh water is released to the salted cavity. The initial temperature and concentration differences, between the salted and the fresh water, are set equal to unity. The thermal boundary condition dictates that no heat is lost to the environment. Therefore, at all sides of the cavity, zero heat flux or temperature gradient normal to the wall is applied. In addition, zero concentration gradient normal to the cavity wall is prescribed. The velocity at all external walls of the cavity are assumed equal to zero. No other boundary condition is required to solve the problem. For the free surface case, the Marangoni boundary conditions are discussed in a later section.

2.2. *Finite element formulations*

The finite element mesh consisted of 5125 nodes. The mesh distribution is shown in Fig. 1. This indicates that the number of grids was increased greatly in the areas where the steepest gradients are expected

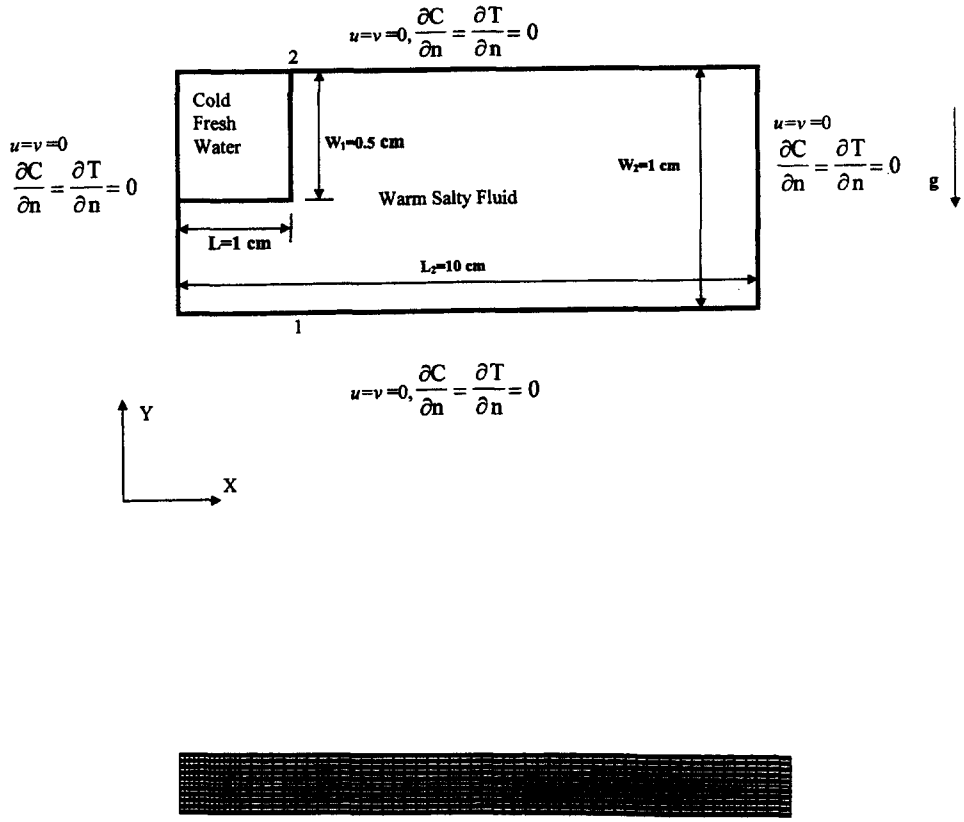

Fig. 1. Finite element model and boundary conditions.

to exist. With this distribution, the total number of grids was found to be adequate. In these elements, velocity, temperature and concentration degrees of freedom were present at each node using the same order of interpolation. The pressure has a bilinear approximation and their degrees of freedom are located at the four points of 2×2 Gaussian integration. The segregated method was used to solve this set of differential equations. At each iteration, the pressure was calculated and a mass adjustment of the velocity field was done. This ensures that the velocity fields satisfy the continuity equation even before convergence is achieved. The solution is assumed to be reached when the following criterion

$$\frac{\|\varsigma_i - \varsigma_{i-1}\|}{\|\varsigma_i\|} \leqslant 0.001$$

is satisfied. The symbol, ς signifies all nodal values of a particular degree of freedom. In the present case, ς consists of the pressure, the two components of velocity, the temperature and the concentration.

This transient problem was solved for different time steps using the backward method with variable time interval. In order to start the calculation with a high accuracy, the first five time steps were fixed for a time interval of 0.001. Above these five time steps, the time interval was variable. For further details of the model see ref. [14].

3. RESULTS AND DISCUSSION

The problem was solved for two different cases. In the first case, the upper horizontal surface (e.g; at $Y = 1$) is assumed to be a fixed wall and the boundary conditions, as shown in Fig. 1, are applied. In the second case, the upper horizontal wall is set to be a free surface in order to study the thermal and solutal interface tension gradient effect and to be closer to Maxworthy's experimental set up that had a free surface.

3.1. *Upper horizontal surface modelled with a rigid wall*

The problem was solved for two different Rayleigh number ($Ra_T = 10^6$ and $Ra_T = 10^4$). This case was close to the one studied by Yoshida *et al.* [10]. Unfortunately, the stream functions and concentration contours of their work did not have any label, making it impossible to compare their work with ours. However, a qualitative comparison was done and results were found to be comparable. Our study is comparable to the case of fixed volume release reported by Maxworthy. A direct comparison of our study with the

results of Maxworthy is made later. The Prandtl number Pr was set equal to 10 (same value Yoshida *et al.* [4] used to model the Maxworthy experiment). The Lewis number Le [$Le = (\alpha_T/\alpha_C) = (Sc/Pr)$] is known to be the ratio of the thermal diffusivity to the solutal diffusivity. In our analysis, two different values of the Lewis number were used ($Le = 1$ and $Le = 100$). In addition, the ratio of the thermal diffusivity in the horizontal and vertical direction was assumed to be equal to unity. Another dimensionless parameter, the Turner number (R_ρ), is the ratio of the salty water density difference to the fresh water density difference. Since the density of the salty water (slower diffusing substance) is written as:

$$\rho_C = \rho_0(1+\beta_C\Delta c)$$

and the density of the fresh water (faster diffusing substance) is written as:

$$\rho_T = \rho_0(1+\beta_T\Delta T).$$

The Turner number (R_ρ) can be written as:

$$R_\rho = [(\rho_C - \rho_0)/(\rho_T - \rho_0)] = (\beta_C\Delta c/\beta_T\Delta T).$$

In our case the Turner number was set equal to unity. Based on the above definition of the thermal Rayleigh number and the solutal Rayleigh number together with the Lewis number and the Turner number, these terms are related as follows:

$$Ra_C = Ra_T \cdot Le \cdot R_\rho.$$

Once the velocities were computed, the stream function ψ was determined using the following well known relationships, $u = (\partial\psi/\partial y)$ and $v = -(\partial\psi/\partial x)$. Stream functions are non-dimensionalised using a reference stream function value given by

$$\psi_0 = L\sqrt{g\beta_T\Delta TL}.$$

Figure 2(a) shows the concentration profiles and the stream line contours for a Lewis number equal to unity and for a thermal Rayleigh number equal to 10^6 at a time $t = 7.5$ s. The intrusion of the salty water into the fresh water is clearly seen in the figure. A descending flow to the bottom of the cavity with increasing salt concentration and ascending salty water with lower concentration to the top of the cavity is observed. The fresh fluid is entrained into the region of salty water creating a backward flow against the main general forward motion of the main intrusion. This phenomenon is similar to the one observed by Maxworthy [3]. Counter-clockwise convection cells are displayed in Fig. 2(a) for the same time step. The Lewis number was set equal to unity, leading to say that the thermal and solutal Raleigh numbers are equal. Since the boundary conditions are the same for both the temperature and the concentration and with a Turner number equal to unity, the two variables, temperature and concentration will have the same profiles. At a later time, the intrusion advances and the convection becomes more noticeable. This is shown in Fig. 2(b), that depicts results after 60 s.

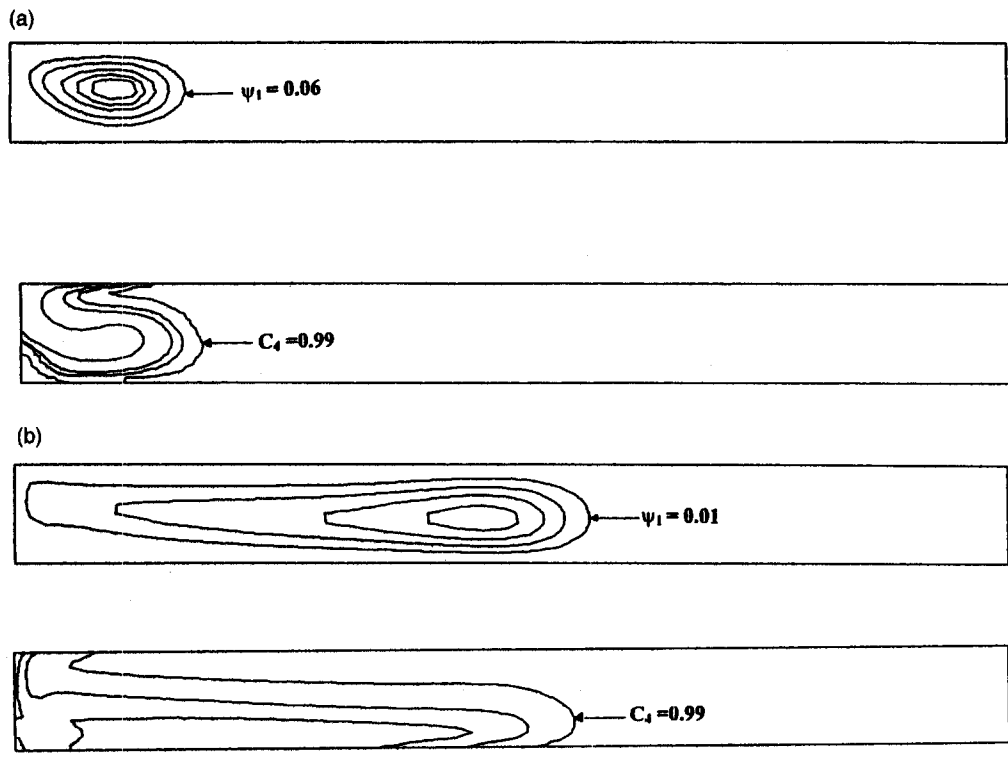

Fig. 2. Stream function and concentration contours ($Le = 1$, $Ra_T = 10^6$, $Ra_C = 10^6$).

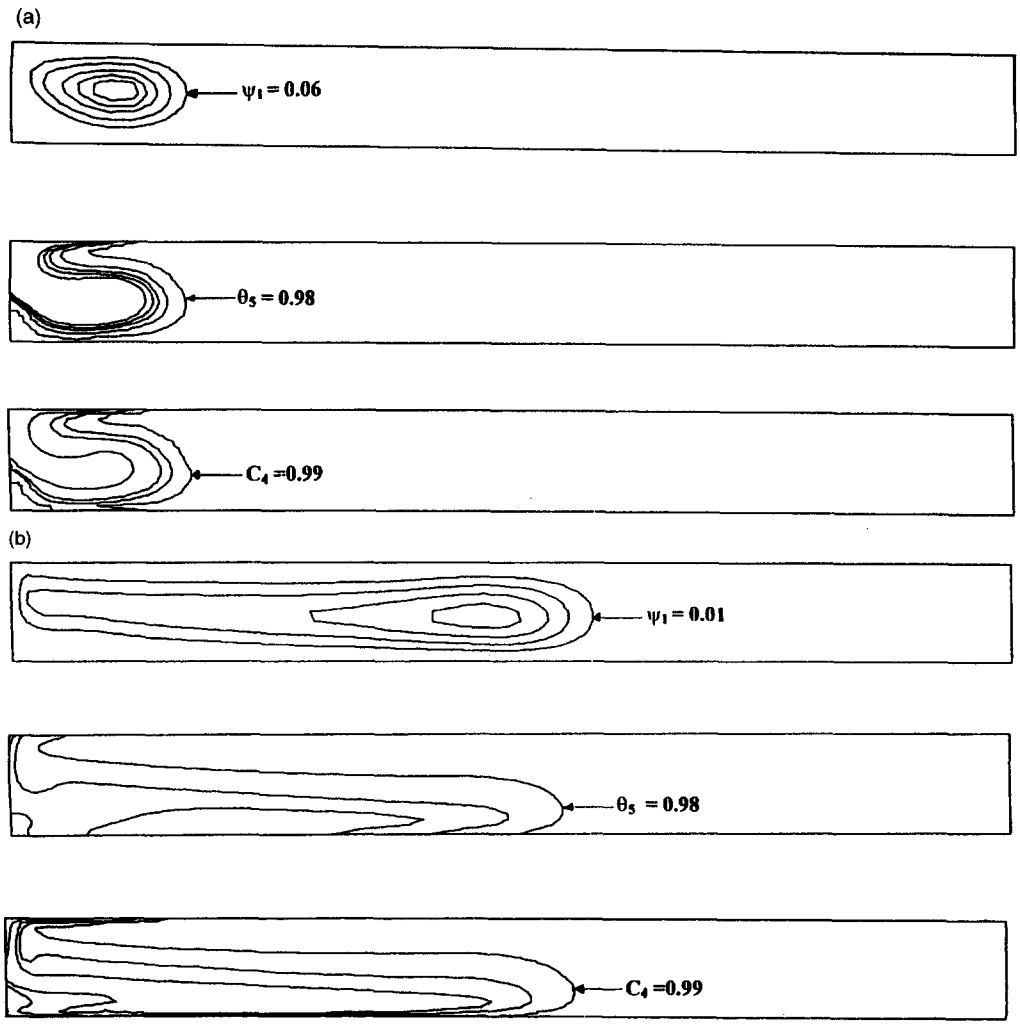

Fig. 3. Stream function, temperature and concentration contours ($Le = 100$, $Ra_T = 10^6$, $Ra_C = 10^8$).

Figure 3 shows the temperature, the concentration and the stream function at various time steps for the case of a Lewis number equal to 100. The temperatures are displayed in a non-dimensional form. Because ΔT is set equal to one, to convert the temperature to a dimensional form, one must add to it the reference temperature, which is 20°C. The solutal Peclet number is 100 times higher than that of the thermal Peclet number. Figure 3(a) shows the concentration/temperature contours and stream functions for a time $t = 7.5$ s. Note that for this early time, there is little difference in these contours from those of $Le = 1$, especially for the concentration/temperature contours. However, the changes occurred for the concentration variables leading to a change in stream functions since the two variables are coupled through the solutal and the Navier–Stokes equations. For this case the temperature and concentration contours are no longer identical. By comparing the concentration contours, one can observe that the shape of contours has evolved. Because a relatively higher Peclet number was used for the latter case, a less steep gradient is formed at the base.

Another way to study the double diffusive effect is by examining the concentration and the temperature profiles at the interface between the fresh water cavity and the salty water cavity. This interface is part of the vertical line located between point 1 ($X = 1$, $Y = 0$) and point 2 ($X = 1$, $Y = 1$) as shown in Fig. 1. Figure 4 displays the concentration and the temperature profiles for the two Lewis numbers used in the model and for a thermal Rayleigh number Ra_T equal to 10^6 and for different time steps. Figure 4(a) shows the temperature profiles for the case of $Le = 1$. The descending flow to the bottom of the cavity and the backflow is clear at time $t = 7.5$ s. As the time increases, the system becomes more stable and the thermal convection becomes more dominant over the solutal convection. By comparing the temperature profiles in Fig. 4 one can see that a distinct cold spot exists only at time $t = 0$ s. As time progresses, the cold spot dissipates to yield to a monotonous variation with

distance, for a time of 60 s. However one cold spot (near the bottom left corner) and a hot spot (near the top right corner) persist.

For the case of $Le = 100$, the double diffusive phenomenon is more obvious. It is interesting to note the shape of the descending flow. A cold high concentration plume, as shown in Fig. 4(b), descends to the bottom of the cavity. At higher time steps (e.g; $t = 60$ s), the concentration profile is still not stable compared to the case of $Le = 1$. At time $t = 7.5$ s, a plumed shape is captured in Fig 4(b) but as the time increases, the thermal convection becomes more dominant. The existence of a solutal hump (at 60 s) is more evident for this case than the one for $Le = 1$. In fact, a modest concentration anomaly persists even at 60 s even though the concentration hump appears to have dissipated away significantly. For the case of $Le = 100$, the temperature profile differs distinctly from the concentration profile. Even though with a Le of 100, a difference is expected, the change in shape is remarkable. At earlier time, the shapes of the concentration and temperature profiles remain very similar. At a later time, however, temperature rises sharply near the base with a distinct thermal hump dominating the flow. For the case of $Le = 100$, no stable profile appears for either concentration or temperature. However, the concentration profile is clearly closer to reaching a stable regime.

Figure 5 shows the velocity vectors for various time steps and for a Lewis number equal to 100. A counterclockwise convection appears as predicted. Beyond the interface, convection does not exist. At time $t = 7.5$ s, a secondary flow appears at the bottom left corner but disappeared at a more advanced time. At a later time, the velocity decreases in magnitude since the thermal effect acts against the diffusive effect. In all cases, single-cell convection persists, however, even at later times, no steady state appears to have taken place.

Figure 6 demonstrates the effect of thermal convection in the system for different values of the Lewis number Le. In this case, the Rayleigh number was set equal to 10^4. As the Rayleigh number decreases, the thermal effect becomes less pronounced, leading to a slower convection. The concentration interface was superimposed to the stream function contour as shown in Fig. 6. For the case of a Lewis number equal to 100, if one compares the concentration contours plot between Figs. 3 and 6 for a time $t = 60$ s, it is obvious that the interface (e.g; $C = 0.99$) has the same

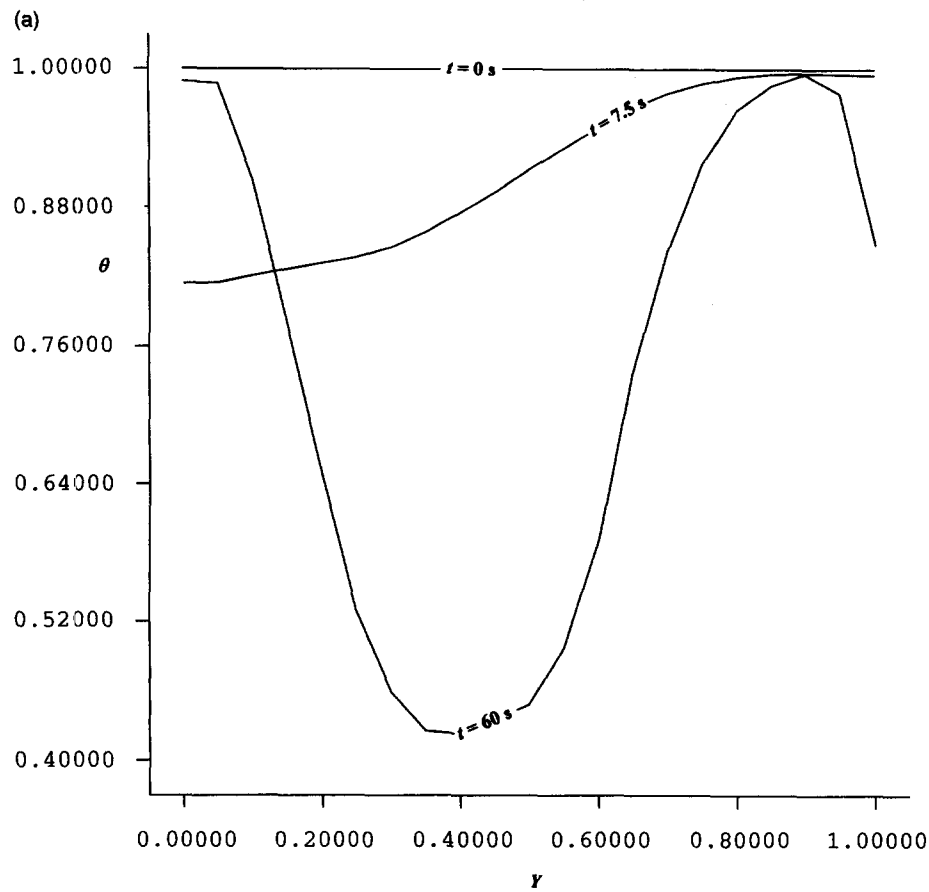

Fig. 4. Concentration and temperature profiles at line 1–2 ($Ra_T = 10^6$).

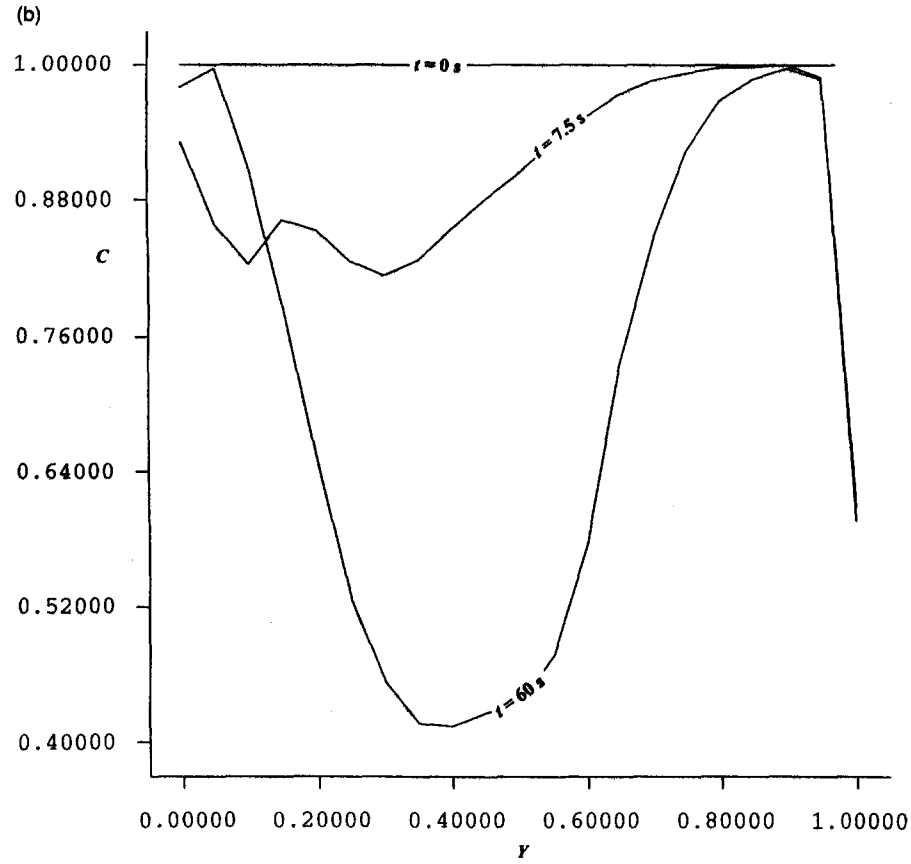

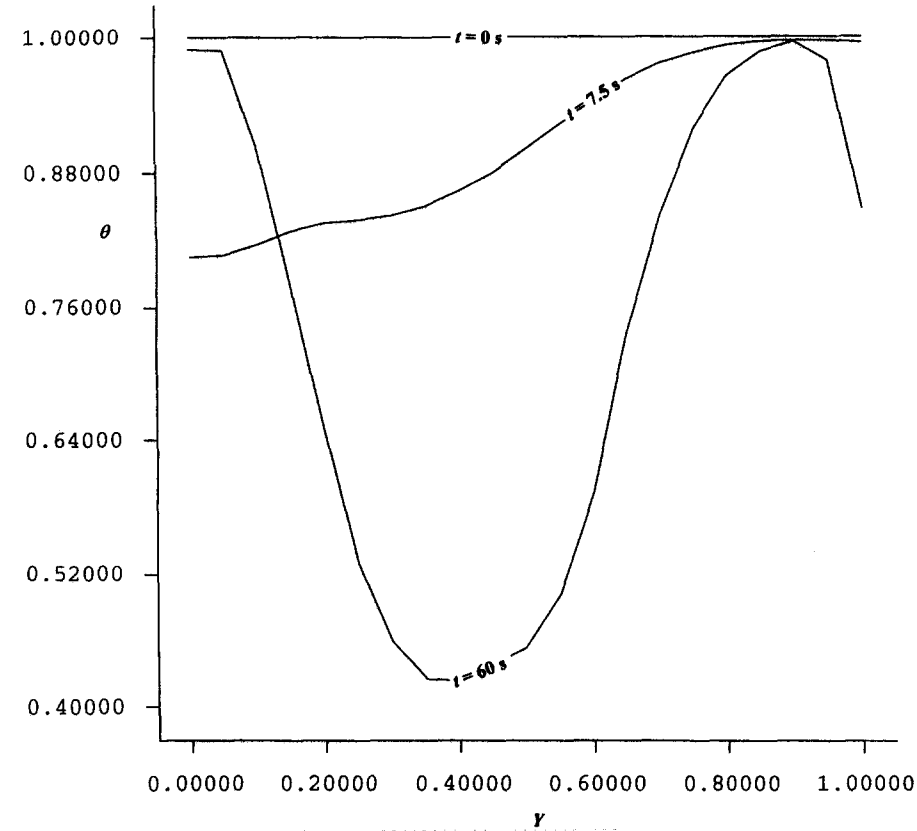

Fig. 4—*continued.*

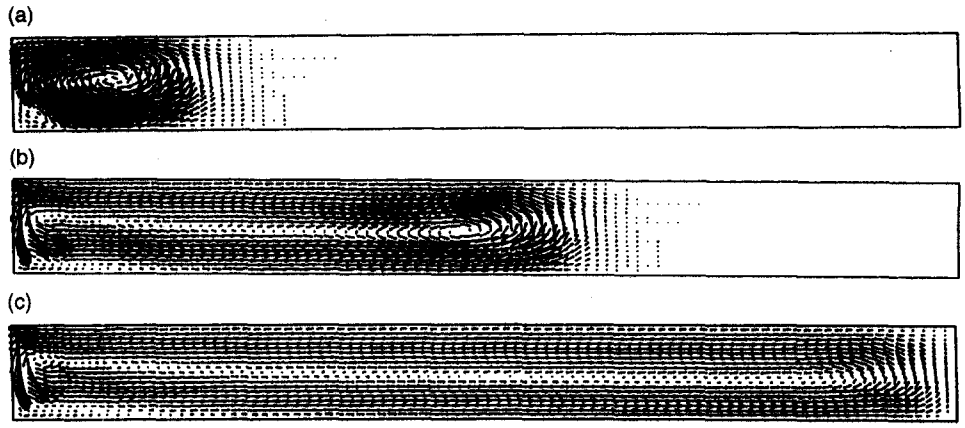

Fig. 5. Velocity vectors for $Le = 100$ ($Ra_T = 10^6$, $Ra_T = 10^8$).

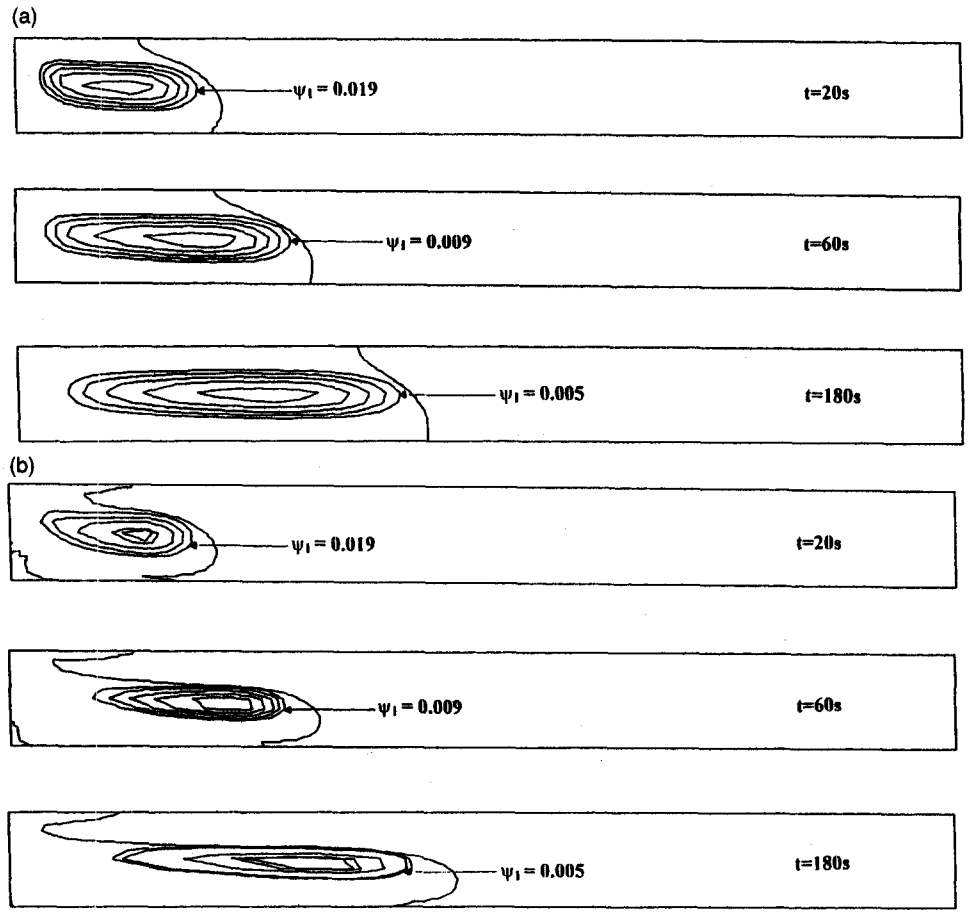

Fig. 6. Stream function and the salinity interface ($Ra_T = 10^4$, $Ra_C = 10^6$).

shape but its spreading rate is higher for higher Rayleigh number. However, for the lower Lewis number ($Le = 1$), the salinity interface has a different shape which is less deformed due to a weaker convection. The thermal and solutal effects enhance the heat and mass exchange in the system leading to a double diffusive phenomenon. By comparing Fig. 6(a) with 6(b), one can see the shaping of the plume. For the case of $Le = 1$, the stream function contour remain blunt whereas, for $Le = 100$, the plume takes shape at a time as early as 20 s.

In order to conduct a direct comparison with the

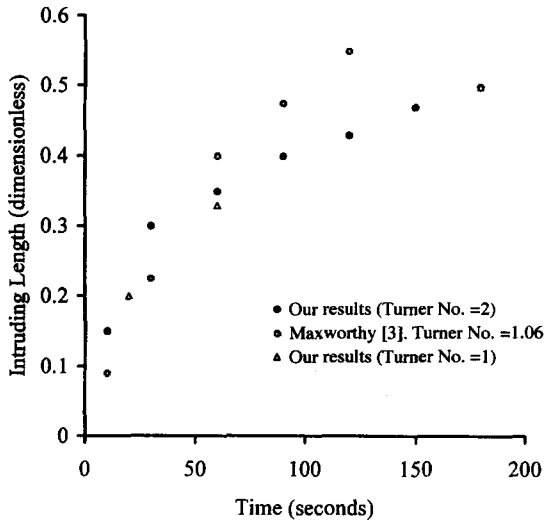

Fig. 7. Variation of the intruding length with time ($Ra_T = 10^6$).

results of Maxworthy [3], the case of fixed volume release was used. Maxworthy used a Turner number of 1.06 for this case. The essential parameter used for comparison was the intruding length as a function of time. In order to facilitate the comparison, the intruding length was non-dimensionalised. Figure 7 compares our results with that of Maxworthy. Excellent match is observed during the early time following the fluid release. Results start to deviate considerably beyond 50 s of the fluid release. Note that the thermal Rayleigh number that we used was 10^4. If a thermal Rayleigh number of 10^6 was used, the agreement at the early phase remains unaffected whereas a much faster intrusion is observed (dimensionless length of 0.56) at a time of 60 s. A closer agreement is observed for the late period by increasing the Turner number to two. Results with a Turner number of two are also shown in Fig. 7. Note that for a Turner number of two, the agreement is somewhat better at the later stage whereas the results remain unchanged at the early stage of fluid intrusion. This relative insensitivity to Turner number was previously observed by Yoshida *et al.* [10]. In summary, Fig. 7 shows that the assumption of no-slip boundary condition is not adequate to capture the movement of the intruding plume at the later stage of the fluid intrusion.

3.2. *Upper horizontal wall is a free surface*

This particular case is closer to the step-up that Maxworthy [3] used in his experiment. He assumed that the surface tension effect at the free surface does not exist. He justified his assumption by indicating that contamination at the free surface removed the surface tension gradient effect. Tanny *et al.* [13] studied the interaction between the double diffusive and the surface tension gradient phenomena by heating the bottom of the cavity. They carefully set up their experiment to avoid any free surface contamination. It is well known that the surface tension varies linearly with temperature and concentration [8, 9]. The thermal Marangoni convection moves fluid at the free surface from low surface tension (high temperature) to a higher surface tension (low temperature). The solutal Marangoni convection moves fluid at the free surface from low surface tension (low concentration) to a higher surface tension (high concentration). The surface tension, σ_m, is defined as:

$$\sigma_m = \sigma_{m0} - \frac{d\sigma_m}{dT}(T - T_0) + \frac{d\sigma_m}{dC}(c - c_0) \qquad (12)$$

where σ_{m0} is the average surface tension at the reference temperature T_0, c_0. Using the same dimensionless variables, as stated earlier, equation (12) becomes:

$$\sigma_m = \frac{1}{Ca} - Ma_T \cdot \theta + Ma_C \cdot C \qquad (13)$$

where the Capillary (Ca) and the Marangoni (Ma_T, Ma_C) numbers are defined as

$$Ca = \frac{\mu u_0}{\sigma_{m0}}$$

$$Ma_T = \frac{|\gamma_T|\Delta T}{\mu u_0} \quad \text{and} \quad Ma_C = \frac{|\gamma_C|\Delta c}{\mu u_0}. \qquad (14)$$

Here γ_T is the thermal surface tension gradient known as $d\sigma_m/dT$ which has a value of -0.1692 dynes cm^{-1} C^{-1}. Also, γ_C is the solutal surface tension gradient known as $d\sigma_m/dc$ which has a value of $+0.367$ dynes cm^{-1} wt%$^{-1}$.

The boundary conditions remain the same as the previous case and only a shear stress at the free surface (equation 13) is included to take into consideration the Marangoni convection. At the free surface the velocity in the x direction is not equal to zero. However, the velocity in the y direction is set equal to zero and therefore, no free surface deformation will occur. Three different cases were studied. In the first case, the effect of the thermal Marangoni convection combined with the double diffusive effect was examined. The solutal Marangoni convection combined with the double diffusive effect was studied in the second case and finally both the thermal and solutal Marangoni convection (e.g. equation 13) combined with the double diffusive convection was studied in detail. In this analysis, the thermal Rayleigh number Ra_T was set equal to 10^4 and the Lewis number was set equal to one.

3.2.1. *Thermal Marangoni convection.* Figure 8 shows the temperature and the velocity profiles at the free surface. As indicated in Section 2.1, the initial temperature boundary conditions was set equal to one in the hot salty water cavity and zero in the cold fresh water cavity. Therefore, at time $t = 0$ s, a zero temperature, at the free surface, is specified in the cold region ($0 \leqslant X \leqslant 1$) and a temperature equal to one is

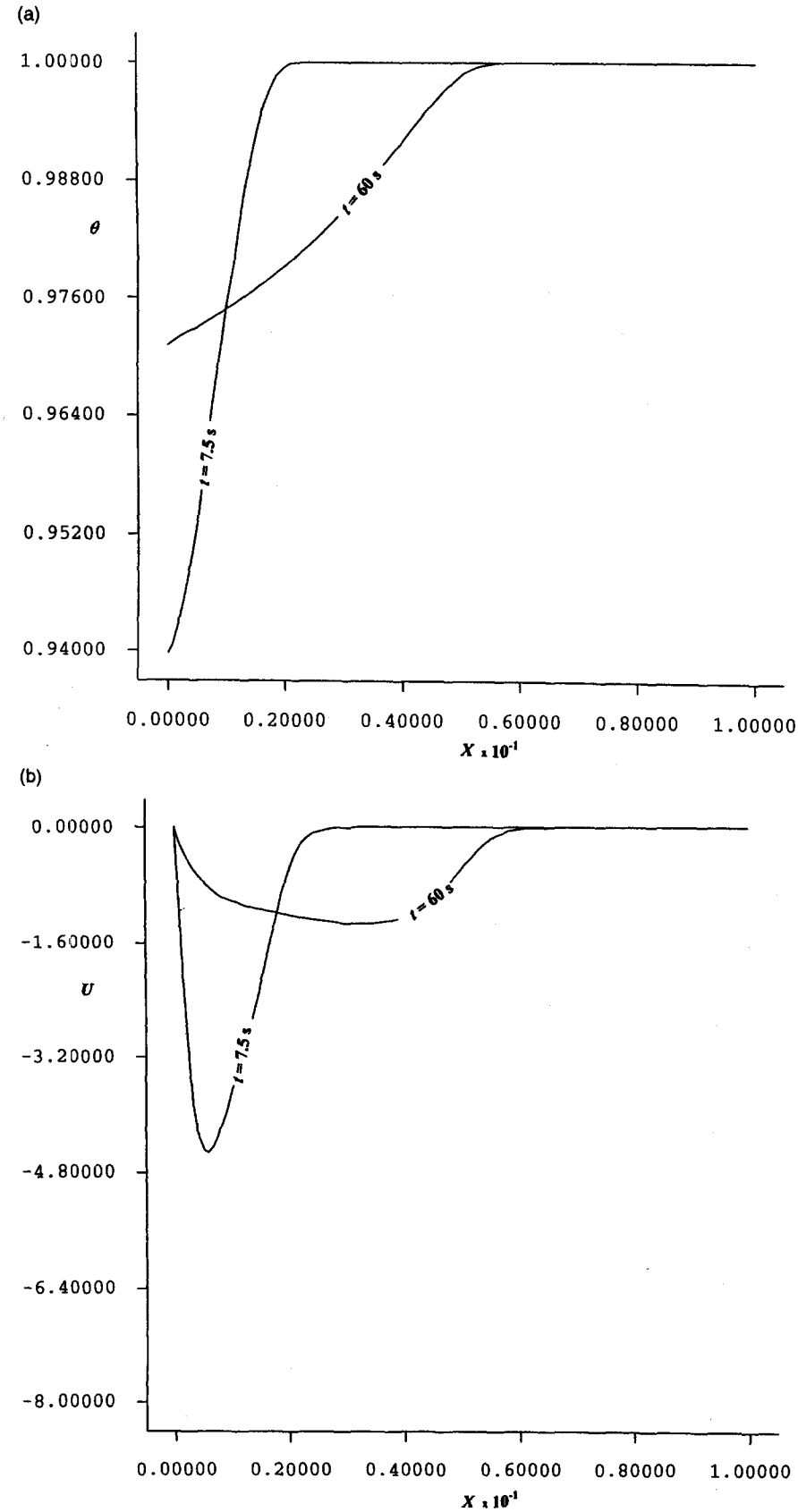

Fig. 8. Temperature and velocity profiles at the free surface due to the thermal Marangoni convection ($Le = 1$, $Ra_T = 10^4$, $Ra_C = 10^4$).

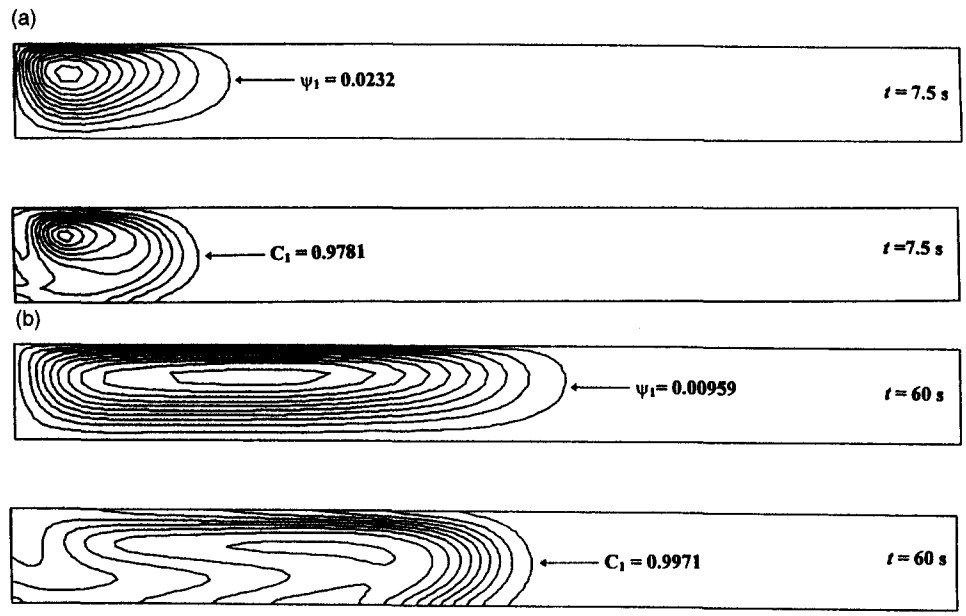

Fig. 9. Stream function and concentration contours due to the thermal Marangoni convection ($Le = 1$, $Ra_T = 10^4$, $Ra_C = 10^4$).

prescribed ($X > 1$, $Y = 1$) in the salty region at the free surface.

As the time increases, the double diffusive convection creates a mixing flow and, therefore, changes the free surface thermal profile as shown in Fig. 8(a) at a time $t = 7.5$ s. The Marangoni convection at that stage becomes effective at a small portion of the free surface as observed in Fig. 8(b) by displaying the velocity in the x direction. A negative velocity indicates a counter-clockwise flow, which adds to the double diffusive convection. This sharp temperature gradient is reduced with time due to the mixing and, hence, the velocity at the free surface becomes smaller. Nevertheless, the convection in the counter-clockwise direction is enhanced as shown in Fig. 8(b). Contrary to the previous case, the temperature/concentration profiles show a smooth profile and the local humps, that were characteristic of the previous case, disappeared. Instead, a more 'dispersion-control' profile appears and the stability is reached without any transitory perturbations. Similar behaviour is observed for the velocity profiles. However, strength of the counter current is higher at the earlier stage. At a later time, the velocity profile becomes blunt and looses strength at the same time.

The stream function and the concentration contours are shown in Fig. 9. By comparing Figs. 6(a) and 9(a), the latter is subject to a stronger flow due to the thermal Marangoni convection. The stream function contours show that strong convective cells are formed from the beginning of the numerical experimentation. At a later time (60 s) the contour shows spreading and assumes an elliptical shape. This is a characteristic of the thermal Marangoni convection. Similar spreading is observed in the concentration contours. However, for a later time, the concentration contour spreads in such a way that the symmetry is lost and local perturbations become prominent at the base.

3.2.2. *Solutal Marangoni convection.* The surface tension gradient depends as explained earlier on the temperature and on the solute gradients. In the temperature case, the gradient is negative. This means that flows will occur from a high-temperature point (lower surface tension) to a lower temperature point (higher surface tension). In the contrary, for the solute case, the surface tension gradient is positive. This indicates that the flow moves from low concentration point (low surface tension) to a higher-concentration point (high surface tension) which is opposite to the thermal Marangoni convection.

Again in this case, the Lewis number is set equal to unity and both the temperature and concentration profiles are the same. This case is different from the previous case that had a different surface tension gradient in sign and magnitude. The initial temperature and concentration profiles remain the same as in the previous case. Figure 10(a) displays the concentration profiles at the free surface at a time $t = 7.5$ s. Different concentration gradients are shown in Fig. 10(a). Figure 10(b) shows the corresponding convective cells of opposite direction at the free surface. Another means of examining the direction of the convective cells is by observing the velocity profiles, as shown in Fig. 10(b). It is worth noting that the velocity is in a non-dimensional form and the reference velocity u_0 is equal to 0.4427 cm s^{-1} [for our case see equation (5)]. As the time increases, the mixing effect

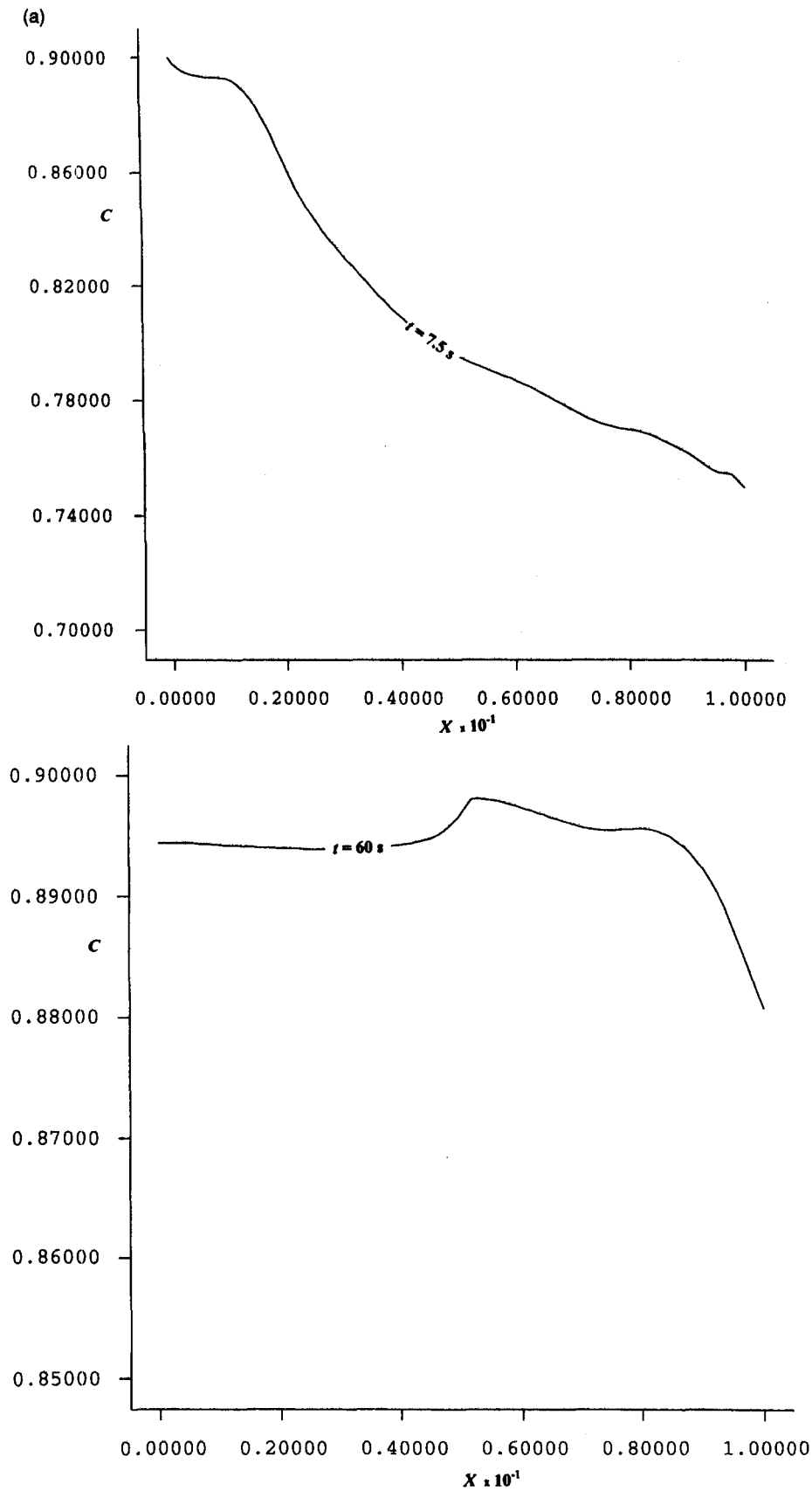

Fig. 10. Concentration and velocity profiles at the free surface due to the solutal Marangoni convection ($Le = 1$, $Ra_T = 10^4$, $Ra_C = 10^4$).

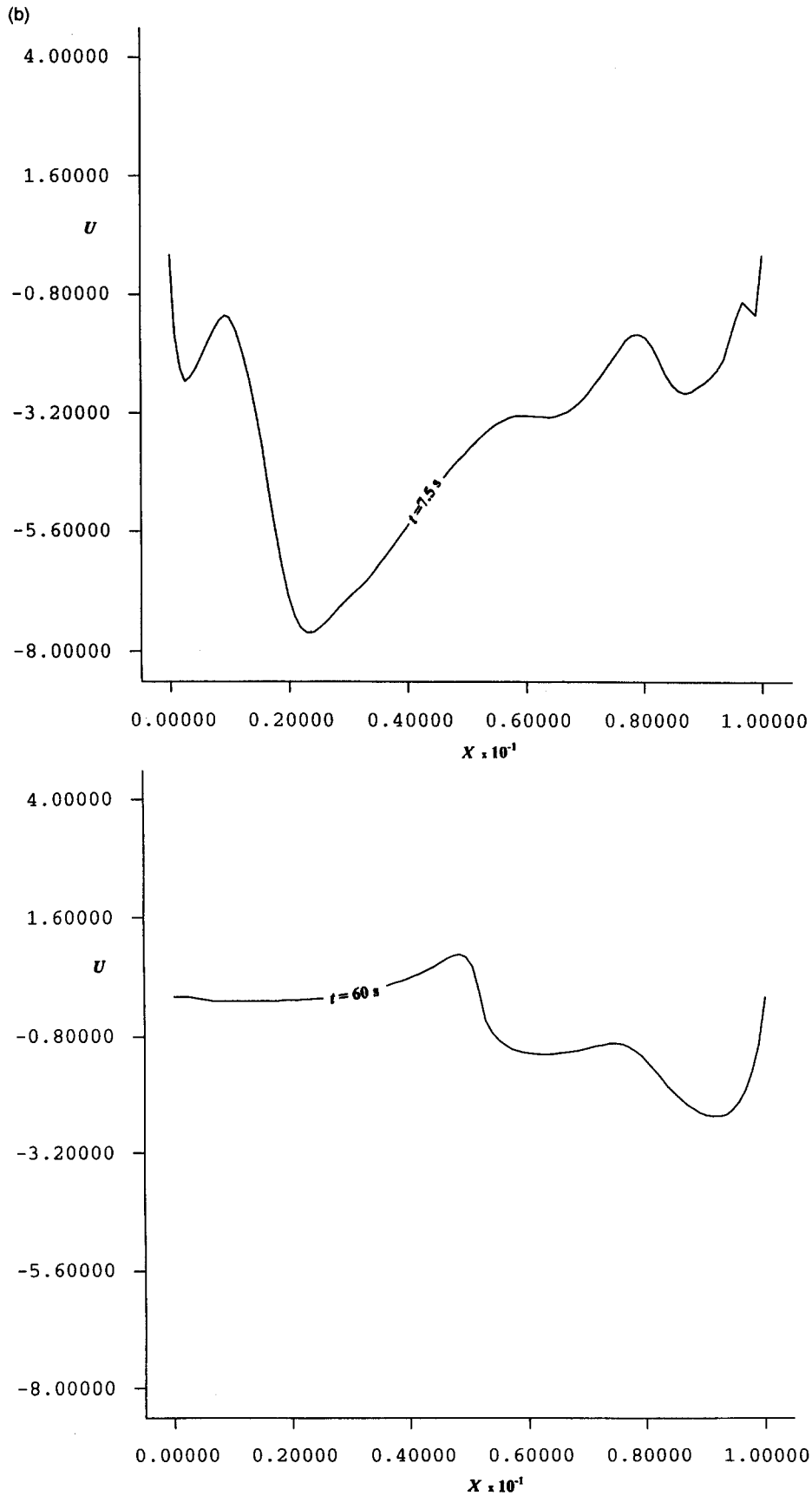

Fig. 10—*continued.*

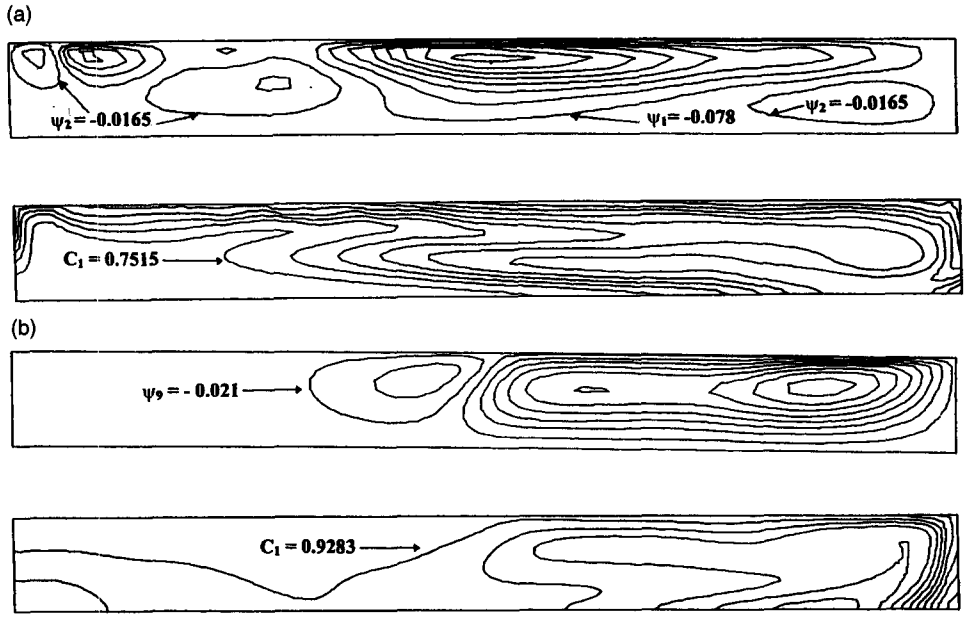

Fig. 11. Stream function and concentration contours due to the solutal Marangoni convection ($Le = 1$, $Ra_T = 10^4$, $Ra_C = 10^4$).

created a more uniform distribution of the solute as shown in Figs. 10(a) and 11(a). This translates into a smoother flow pattern as shown in Figs. 10(b) and 11(b). It is clear that the solutal Marangoni convection has enhanced the mixing in the cavity and has created smaller convective cells. The flow is some agitated than in the case of the thermal Marangoni convection.

3.2.3. *Combined thermal and solutal Marangoni convection.* In order to reach a more realistic case, both thermal and solutal Marangoni convections were included in the model. In the previous case, the effect of each term of the Marangoni convection was studied separately. The model was repeated by combining both effects for the case of a Lewis number, $Le = 1$ and a thermal Rayleigh number, $Ra_T = 10^4$. Figures 12 and 13 display the concentration, the velocity at the free surface and the stream function contour plots. The stream function contours indicate that the intense cellular pattern that was initiated by invoking solutal Marangoni effect, has been subsided significantly. However, the number of cells remains high as compared to the case of thermal Marangoni convection (see Fig. 9). The general profile of the concentration contours is similar to the one observed with solutal Marangoni convection. However, the flow is tangibly less intense. The competing forces of surface tension and double diffusion gives rise to the smearing of the concentration profile. Such smearing is absent in the presence of uniquely thermal Marangoni effect. The thermal Marangoni number Ma_T was equal to 27 and the solutal Marangoni number Ma_C was equal to 59. Based on the work done by Chen and Su [12], for the chosen Marangoni numbers, the flow is always located in the stable regime. Referring back to the Maxworthy experiment, one can see that even if the experiment had thermal Marangoni effect, a change in the concentration profile would not be detected. The solutal Marangoni effect, on the other hand, would have made the concentration plumes propagate differently than the one observed. It can be said that the solutal Marangoni convection was negated by the contamination of the free surface in the Maxworthy experiment.

4. CONCLUSIONS

In this study, the importance of the interaction between the double diffusive convection and the Marangoni convection in the intrusion process is demonstrated. It is shown that the double diffusive convection plays a major role in the intrusion of the salted water into fresh water. Besides temperature, salinity induces a strong convection. In addition, if a free surface exists in the system, another surface force, namely the thermal and solutal Marangoni convection, enhances this convection. The role and the interactions among different parameters, mainly the thermal Rayleigh number, the thermal and solutal Marangoni numbers on the convection scheme were demonstrated. Based on the numerical study of the experimental model of Maxworthy, it is concluded that surface forces should not be ignored but should be taken into consideration during the numerical analysis. However, as per the analysis of Maxworthy, his experimental set-up indeed lacked tangible influence of the solutal Marangoni convection.

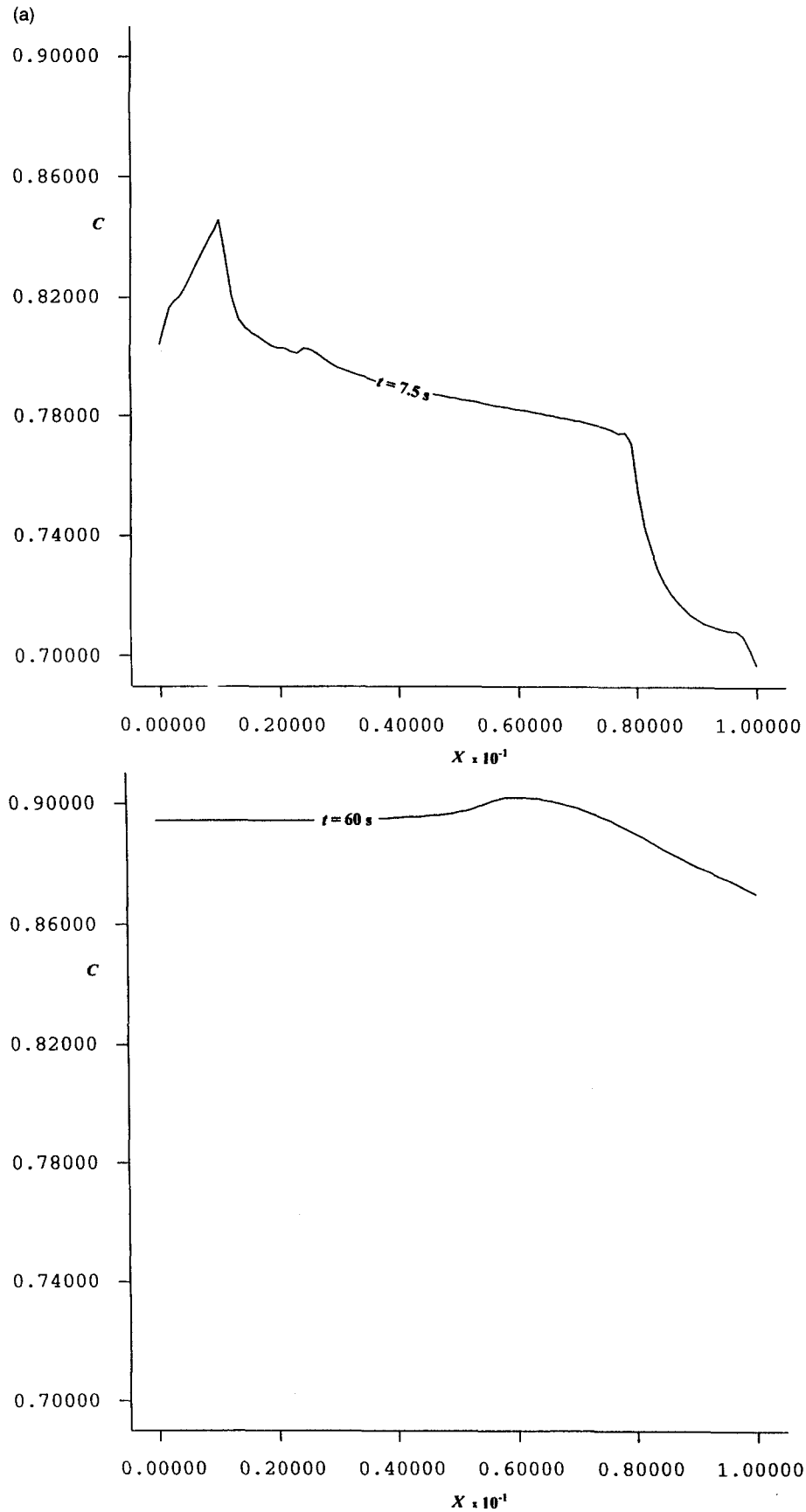

Fig. 12. Concentration and velocity profiles at the free surface due to the thermal and the solutal Marangoni convection ($Le = 1$, $Ra_T = 10^4$, $Ra_C = 10^4$).

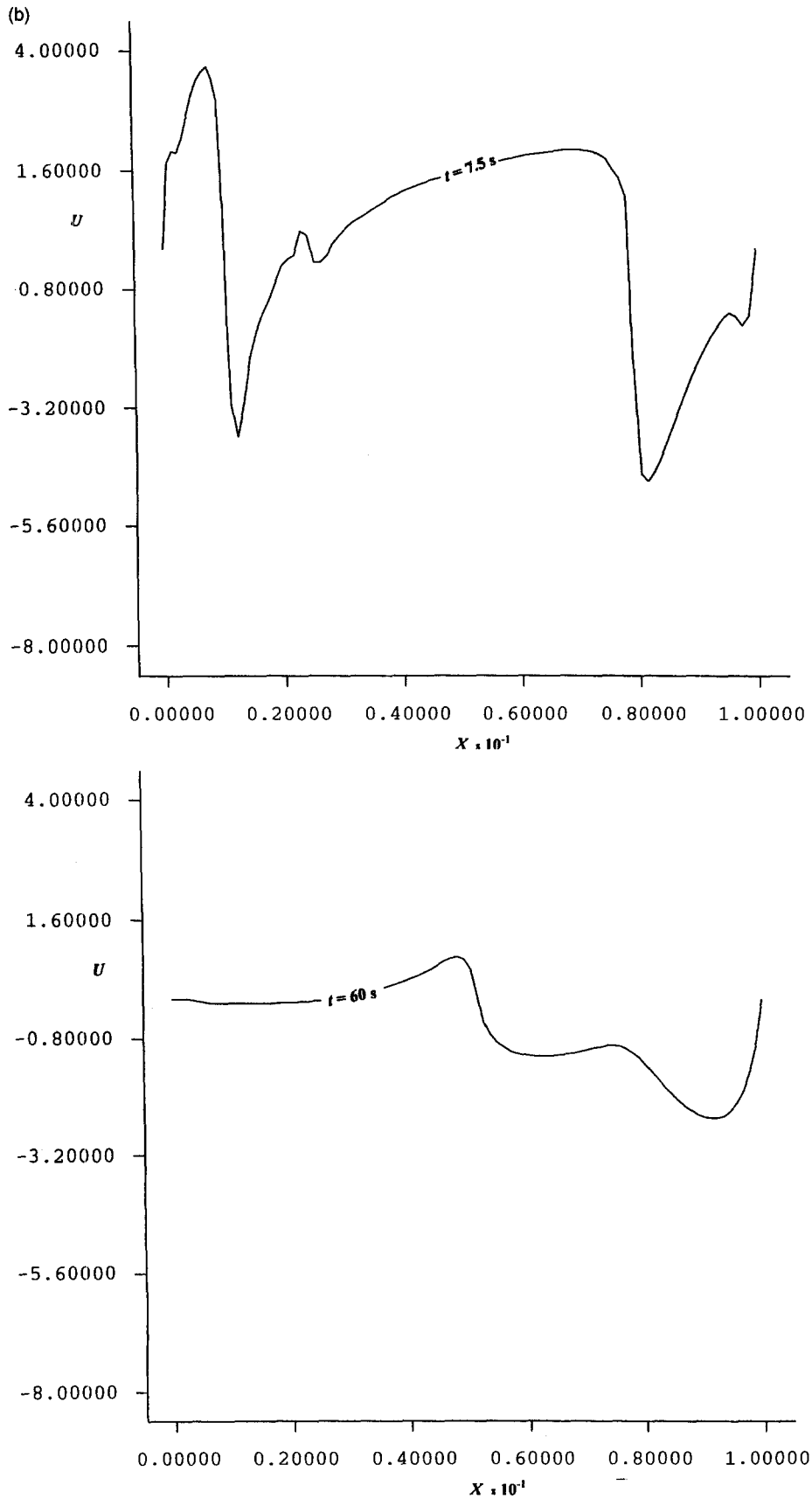

Fig. 12—*continued.*

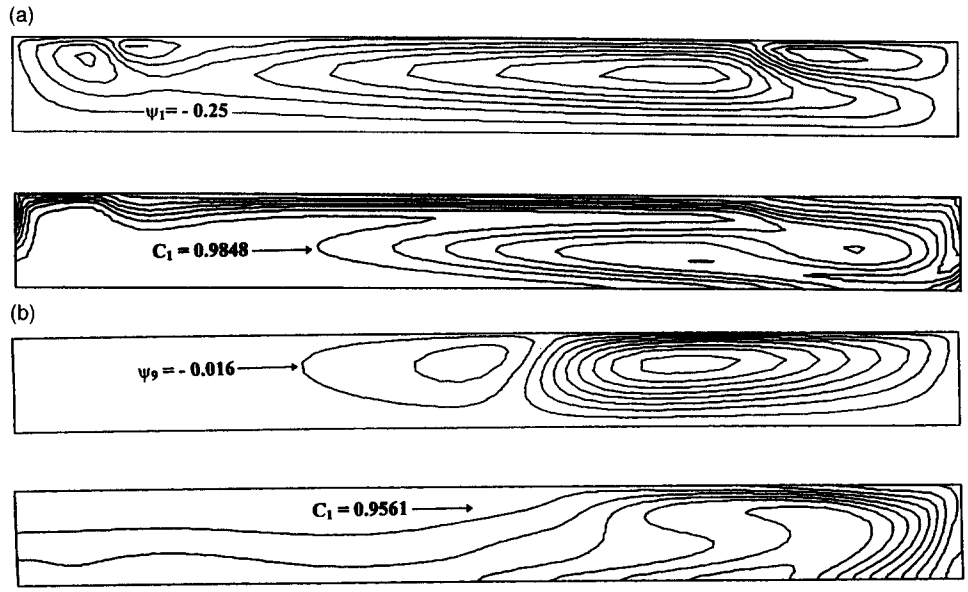

Fig. 13. Stream function and concentration contours due to the thermal and the solutal Marangoni convection ($Le = 1$, $Ra_T = 10^4$, $Ra_C = 10^4$).

Acknowledgement—The authors would like to acknowledge the financial support of Zayed International Agriculture and Environmental Research Program.

REFERENCES

1. Chen, F. and Chen, C. F., Double-diffusive fingering convection in a porous medium. *International Journal of Heat and Mass Transfer*, 1993, **36**(3), 793–807.
2. Thangam, T. and Chen, C. F., Salt-finger convection in the surface discharge of heated saline jets. *Geophy. Astrophys. Fluid Dyn.*, 1981, **18,** 111–146.
3. Maxworthy, T., The dynamics of double diffusive gravity currents. *Journal of Fluid Mechanics*, 1983, **128,** 259–282.
4. Yoshida, J., Nagashima, H. and Nagasaka, M., A double diffusive lock-exchange flow with small density difference. *Fluid Dynamics Research*, 1987, **2,** 205–215.
5. Schmitt, R. W., Why didn't Rayleigh discover salt fingers? *Double Diffusive Convection Geophysical Monograph*, 1994, **94,** 3–10.
6. Ruddick, B. and Turner, J. S., The vertical length scale of double-diffusive intrusions, *Deep Sea Research*, 1979, **26,** 903–913.
7. Thamgan, T. and Chen, C. F., Salt-finger convection in the surface discharge of heated saline jets. *Geophys. Astrophys. Fluid Dyn.*, 1981, **18,** 111–146.
8. Li, J., Sun, J. and Saghir, M., Buoyant and thermocapillary flow in liquid encapsulated floating zone. *Journal of Crystal Growth*, 1993, **131,** 83–96.
9. Saghir, M. Z., Abbaschian, R. and Raman, R., Numerical analysis of thermocapillary convection in axisymmetric liquid encapsulated InBi. *Journal of Crystal Growth*, 1996, **169**(1), 110–117.
10. Yoshida, J., Nagashima, H. and Nagasaka, M., Numerical experiment on double diffusive currents. *Double Diffusive Convection Geophysical Monograph*, 1994, **94,** 69–79.
11. Hyun, M. T. and Bergman, T. L., Direct simulation of double diffusive layered convection. *Transaction of the ASME*, 1995, **117,** 334–337.
12. Chen, C. F. and Su, T. F., Effect of surface tension on the onset of convection in a double-diffusive layer. *Physics of Fluids A*, 1992, **4**(11).
13. Tanny, J., Chen, C. C. and Chen, C. F., Effects of interaction between Marangoni convection and double diffusive instabilities. *Journal of Fluid Mechanics*, 1995, **303,** 1–21.
14. Saghir, M. Z., Abbaschian, R. and Raman, R., Numerical analysis of thermocapillary convection in axisymmetric liquid encapsulated InBi. *Journal of Crystal Growth*, 1996, **169,** 110–117.